ORIGINAL RESEARCH

Synthesis of nanocrystalline cellulose via ammonium persulfate-assisted swelling followed by oxidation and their chiral self-assembly

Hong Wang · Manoj Pudukudy · Yonghao Ni · Yunfei Zhi · Heng Zhang · Zhenquan Wang · Qingming Jia · Shaoyun Shan

Abstract A single-step ammonium persulfate (APS)-assisted swelling, followed by oxidation, can prepare nanocrystalline cellulose (NCC) from cotton linters. The APS-swelling is the critical step in the process, and the effects of swelling time, temperature and solid–liquid ratios were thoroughly investigated. The optimal conditions for NCC preparation were a swelling time of 3.0 h, a swelling temperature of 25 °C, and a solid–liquid ratio of 1:50. Upon heating at 60 °C, the persulfate enters the amorphous region of the cellulose and produces active SO_4^- and H_2O_2, which effectively attack the two-phase structure of cellulose and oxidize the –OH group at the C-6 position. The swelling temperature of 25 °C plays a crucial role in breaking the hydrogen bonds between the molecular chains of cellulose. It permits the preparation of NCC with a high yield and crystallinity index. The crystalline structure of cellulose I_β did not change after APS swelling and oxidation. The atomic force microscopic analysis confirmed the formation of spindle-shaped particles with a helical structure. Upon natural evaporation of the NCC suspension, brittle films were obtained, which exhibited a left-hand layered structure and high iridescence with a fingerprint-texture. These materials can be applied as strength additives and chiral templates.

H. Wang · M. Pudukudy · Y. Zhi · H. Zhang · Q. Jia (✉) · S. Shan (✉)
Faculty of Chemical Engineering, Kunming University of Science and Technology, Kunming 650500, Yunnan, People's Republic of China
e-mail: jiaqm411@163.com

S. Shan
e-mail: shansy411@163.com

Y. Ni
Limerick Pulp and Paper Centre, University of New Brunswick, Fredericton E3B5A3, Canada

Z. Wang
Faculty of Environmental Science and Engineering, Kunming University of Science and Technology, Kunming 650500, Yunnan, People's Republic of China

Graphic abstract
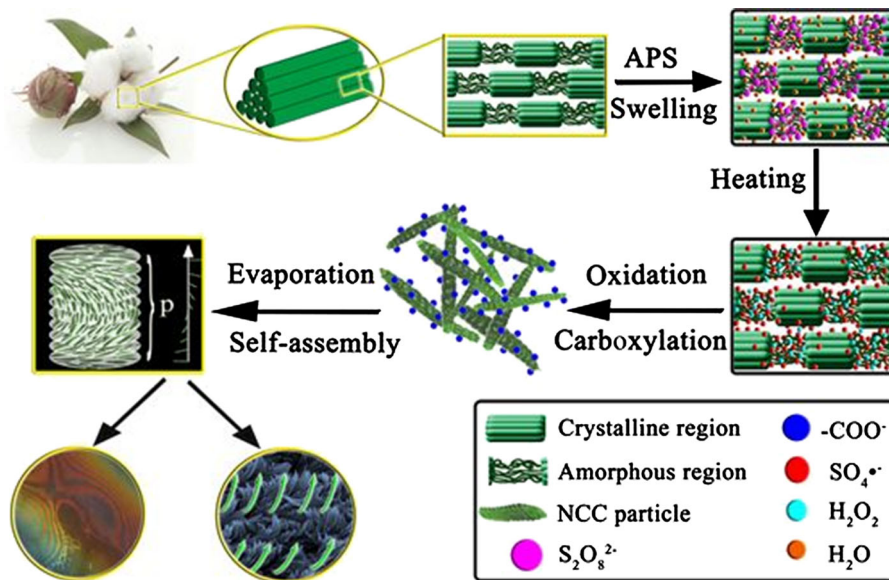
Keywords One-step synthesis · Nanocrystalline cellulose · Ammonium persulfate · Swelling · Oxidation · Spindle-shaped helical structure · Chiral self-assembly

Introduction

Nanocrystalline cellulose (NCC) is produced from cellulose mainly via acid hydrolysis, oxidation, enzymatic and mechanical processes and their combinations. NCC is one of the most abundant resources and most important renewable polymers on earth (Klemm et al. 2005). NCC has several advantages including a high aspect ratio, large surface area and tremendous stiffness (Jackson et al. 2011; Xu et al. 2016). Simultaneously, it is not only biocompatible and biodegradable, but it is also green and sustainable. Therefore, NCC has attained an increased interest in the fields of reinforcement in polymer composites and its self-assembly. It is found numerous applications in the fields of security printing (Chindawong and Johannsmann 2014), enzyme immobilization (Mahmoud et al. 2009), drug delivery excipients (Jackson et al. 2011; Mohanta et al. 2014), bio-imaging (Dong and Roman 2007), solar energy harvesting (Fang et al. 2014), tissue engineering (Domingues et al. 2014),

electronics (Huang et al. 2013), bio-sensing materials (Mohanta et al. 2014; Ooi et al. 2016), biodegradable films (Huq et al. 2012), chiral templates (Asefa 2012; Shopsowitz et al. 2010), optical materials (Yang et al. 2012), etc.

The use of sulfuric acid to produce NCC has been well established because it imparts sulfate groups on the NCC surface, and these sulfonic groups are responsible for the stable aqueous NCC suspensions (Abitbol et al. 2013; Revol et al. 1992). However, there are two problems associated with the sulfuric acid hydrolysis method: (1) the thermal stability of resultant NCC is poor, and (2) a very high concentration of sulfuric acid (usually 64 wt%) is required, which leads to challenges in the processing equipment and overall operation process and the production of a large amount of waste acid, which is difficult to dispose of.

Mechanical methods, such as ball milling or a homogenizer, are also commonly used methods to prepare NCC. However, the mechanical method has the disadvantages of high equipment cost and high energy consumption. It is usually used in combination with chemical methods to reach the targeted properties (Cheng et al. 2016; Cui et al. 2016; Lee et al. 2018; Lu et al. 2016a). The hydroxyl group on the surface of cellulose is highly reactive for the oxidative degradation and is therefore easily oxidized into carboxyl

groups by strong oxidants (Potthast et al. 2006). Even these oxidants can destroy the structure and reduce the degree of polymerization; they are effective for increasing the surface areas of cellulose materials, thus facilitating the formation of nanocrystalline cellulose.

Carboxylated NCC is reported to be fabricated by the 2,2,6,6-tetramethylpiperidine-1-oxyl radical (TEMPO) oxidation method (Isogai et al. 2011; Montanari et al. 2005) and deep eutectic solvent (DES) treatment, which results in the formation of a stable NCC suspension. The TEMPO oxidation method also has several limitations such as toxicity, high costs (Carlsson et al. 2014; Saito and Isogai 2004), and a long preparation time (Lin et al. 2012), and it still results in the limited oxidation of cellulose at C-6 hydroxyl groups (Batmaz et al. 2014). Although the DES treatment can prepare the NCC with a length distribution of 50-500 nm and a width of 3–5 nm, it belongs to the ionic liquids (ILs) category with high cost (Chen et al. 2015). It also requires the use of a catalyst (Yang et al. 2019) or two-step methods including DES pre-treatment and mechanical disintegration using micro fluidizer (Sirviö et al. 2016) or ultrasonic treatment (Liu et al. 2017; Ma et al. 2019) to improve the yield and crystallinity index.

In an early study (Cheng et al. 2014), ammonium persulfate (APS) was used as an oxidant in the hydrolysis of lyocell fibres to produce spherical cellulose nanocrystals (SCNCs), which are of cellulose II crystalline structure, possibly because lyocell fibres, a type of re-generated cellulose, are the raw material. In the process, carboxyl groups are formed from the oxidation of hydroxyl groups at the C-6 position. APS oxidation is a cost-effective and environmentally friendly method that also offers mild oxidation conditions (Castro-Guerrero and Gray 2014; Leung et al. 2011). The bond of –O–O– in APS is unstable and is readily decomposed into hydrogen peroxide (H_2O_2) and radical ($SO_4 \cdot ^-$) (Liu and Wang 2014; Schneider et al. 2001; Wang et al. 2016), which has a strong oxidizing capacity.

The amorphous region of cellulose is loose and has a large molecular distance; thereby, it can be readily accessible by the reactants. The crystalline region of cellulose is compact, highly ordered, and has a small molecular space (Gardner and Blackwell 1974). Thus, it is not as accessible by the oxidants. Although the usage of APS volume is large, the yield of the

preparing nanocrystalline cellulose is not high because of the two-phase structure of cellulose. Therefore, corresponding measures must be taken to solve these issues. As reported, several solvents can form hydrogen bonds in the amorphous region of cellulose to swell and affect the crystallization region of the cellulose (Mantanis et al. 1995). The rapid swelling of natural and regenerated cellulose in aqueous medium is an effective method for cellulose activation (Cuissinat and Navard 2006; Mantanis et al. 1994; Röder et al. 2001).

An effective diffusion of oxidants, such as APS and the associated active oxidative species, into the cellulose structure is paramount in using APS to prepare NCC from cotton linters (Leung et al. 2011). The hypothesis of the present study is to allow optimal swelling of cotton linters in the presence of APS solution, which will have a significant impact on the quality of resultant NCC and the overall process, such as the yield and crystallinity index.

Herein is the first proposal of a novel method of preparing NCC from cotton linters using APS in a one-pot process that allows the swelling of cellulose raw materials in the APS solution, followed by oxidation. In this study, the effects of swelling time, swelling temperature and solid–liquid (S–L) ratios were investigated in detail. To the best of our knowledge, no similar reports are available in the literature.

Experimental section

Materials

Cotton linters with a cellulose content of more than 95% were purchased from Hubei Chemical Fiber Co. Ltd. (Xiangfan, China). The cotton linters were used without further purification. Ammonium persulfate was purchased from Aladdin Industrial Corporation (Shanghai, China). Deionized water was used in all the experimental studies.

Preparation of NCCs and films

A schematic representation of the synthesis procedure is shown in Fig. 1. In a typical procedure, 5 g of cotton linter pieces was subjected to swelling in a 500 mL 1.5 mol/L aqueous solution of APS at different swelling times (0.0, 0.5, 3.0 and 6.0 h) and different
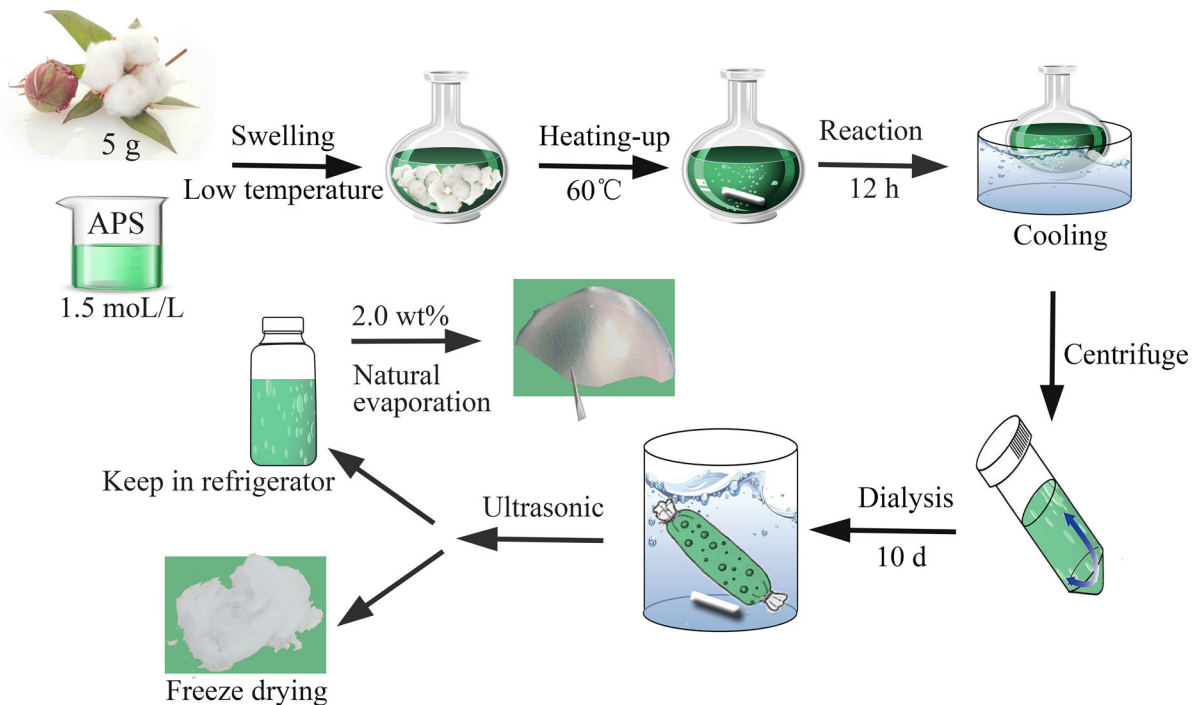
Fig. 1 Schematic representation of the preparation of NCC by APS swelling followed by oxidation, and NCC films

swelling temperatures (− 15, − 5 and 25 °C) with homogenous mixing. After the swelling, the system was heated to 60 °C and kept for the oxidation reaction under continuous stirring in the dark for 12.0 h. Once the reaction finished, the solution was kept in a 10 °C ice bath to terminate oxidation. Then, the supernatant solution was removed, and the remaining sediment was kept as such until reaching a transparent and stable suspension by repeated centrifuge cycles (10 min at 10,000 rpm). The transparent NCC suspensions were collected from the upper layer until the supernatant liquid was cloudy. The NCC suspensions were then dialysed for approximately 10 days until the pH was consistent with that of deionized water. To obtain homogeneous and well-dispersed suspensions, the NCC suspensions were ultrasonicated for 10 min at 60% amplitude with a pulse of 2 s on and 1 s off. Finally, a part of the NCC suspensions was concentrated to 2.0 wt% and stored in the refrigerator whereas part of the NCC suspensions was freeze-dried for subsequent characterization. After obtaining the optimal swelling time and temperature, the effect of various S–L ratios (1:40, 1:50, 1:75, and 1:100) was investigated. The final products were named SNCC-x after different swelling and oxidation reaction conditions. A hydrophobic glass Petri dish with an inner diameter of 60 mm was filled with 2.0 wt% 45 mL of the well-dispersed NCC suspension, and the water was evaporated to obtain NCC films on the hydrophobic surface at room temperature.

Materials characterization

Optical microscopy measurements

The raw and dispersed cotton linters with different swelling times and temperatures were placed in between two glass plates and viewed under a Leica DM1000 optical microscope (Wetzlar, Germany) in transmission mode. The images were obtained using a high-resolution single-CCD camera. The width distribution results of the cotton linters were obtained from the optical images using the ImageJ V.1.8.0 software, and the data were imported to Origin 8.0. The average value and error scale was considered through the data analysis function using statistics on columns and frequency counts. More than 100 points were considered to report the results.

Yield of nanocrystalline cellulose (NCC)

The NCC yield (%) (Kian et al. 2018; Lu et al. 2016b) was calculated using the following equation:

$$Yield(\%) = \frac{(M_2 - M_3) \times V_2}{M_1 \times V_1 \times 95\%} \times 100\%$$

where M_1 represents the mass of cotton linters; M_2 represents the total mass of freeze-drying NCC in the weighing bottle; M_3 represents the mass of the weighing bottle; V_1 represents the volume of NCC suspensions subjected to freeze-drying; V_2 represents the total volume of collected supernatant NCC suspensions; and 95% represents the content of cellulose in the cotton linters.

X-ray diffraction (XRD) analysis

The crystalline phases of the NCC samples were obtained by X-ray diffraction (XRD) measurements on an X'Pert3 powder diffractometer (PANalytical Co. Ltd. Netherlands) with CuKα radiation ($\lambda = 1.5406$ Å), operated at 40 kV and 40 mA. The scattered radiation of intensity was recorded at ambient conditions in the range of 2θ from 4° to 50°. The crystallinity index (CI) of each NCC sample was calculated using the method described by Segal et al. (1959):

$$CI = \frac{I_{200} - I_{am}}{I_{200}} \times 100$$

where I_{200} is the intensity of the peak at (200) plane for the crystalline regions of cellulose I_β (2θ = 22.7°), and I_{am} is the minimum intensity for the amorphous regions of cellulose I_β (2θ = 18.7°).

Fourier transform infrared spectroscopy (FT-IR)

The Fourier transform infrared spectra (FT-IR) of the NCC sample were assessed using Bruker Vertex 70 (Bruker Spectroscopy Corp., Germany). The test NCC sample slices were prepared by mixing the freeze-dried NCC with anhydrous KBr and pressing in a bead machine. The spectral range was from 500 to 4000 cm^{-1}.

Degree of polymerization (DP)

In this method, 25 mL of distilled water was added to the viscosity bottle containing cotton linters and/or NCC samples (0.1 g), and 2–3 copper sheets were added to it, followed by a slight agitation to separate the cellulose. Next, 25 mL of copper (II) ethylenediamine (cuene) solution was added to the bottle, and small glass beads were also added to drain the air. The bottle was then shaken vigorously by hand to make the sample completely slushed. A certain amount of sample-cuene solution was then transferred into a Pinkevitch viscometer and placed vertically in a measuring device at a constant temperature of 25 °C, where it remained standing for 10 min. The time required for the solution to fall freely between the two marks was measured. The DP was then determined from the following formula (Immergut et al. 1953):

$$DP^{0.905} = 0.75[\eta]$$

where DP is the initial DP of cellulose, and $[\eta]$ is the intrinsic viscosity in mL/g. The average value of three repeated tests was reported.

Zeta potential

The zeta potential of the NCC suspensions was measured by dynamic light scattering (DLS) using a Zeta potential analyser (Zetasizer Nano ZS, Malvern, UK). The NCC suspension with a mass concentration of 0.05 wt% was ultrasonically dispersed for 5 min. Each sample was tested 3 times, and the arithmetic mean value was taken.

Thermo-gravimetric analysis (TGA)

The thermal stability of the NCC samples was determined by means of a thermo gravimetric analyser using a NETZSCH STA 449F3@Jupiter (Germany) at a heating rate of 10 °C under nitrogen atmosphere from 20 °C to 600 °C.

Atomic force microscopy (AFM)

The morphology of NCC was characterized by AFM. The sample was prepared in a freshly cleaved mica substrate, which was dipped in a dispersed NCC suspension with a mass concentration of 0.05 wt% for

5 min and dried in nitrogen flux for 2.0 h. The AFM images were collected in a Peak Forcing Tapping of the Bruker MM8 system with a silicon probe having Al-Reflex coating on the tip and a resonance frequency of 70 kHz. Ra is the mean roughness, the arithmetic average of the absolute values of the NCC surface height deviations, calculated by the Research NanoScope Analysis software. The length and diameter distribution of NCC were obtained from the AFM images using ImageJ V.1.8.0 software, and the data were imported to Origin 8.0. Their average value and error scale was considered through the data analysis function using statistics on columns and frequency counts. Nearly 300 points were considered to report the data.

Polarized optical microscopy (POM)

The NCC films were placed in between two glass plates and viewed under an Olympus BX51 advanced Polarizing Microscope (Japan) in reflection mode with crossed polarizers.

Field emission scanning electron microscopy (FESEM)

The cross-sections of the NCC films were fixed with conductive adhesives on a special test aluminium table and then sprayed with gold. Secondary electron (SE) cross-sectional morphology images of the NCC films were studied with the Nova NanoSEM 450. Under the highly vacuumed environment, the accelerating voltage of FESEM imaging was 5 kV, and the working distance was 5.0 mm.

Results and discussion

Effect of cotton linter swelling at different times and temperatures

Figure 2 shows the optical micrographs of the cotton linter samples at different swelling times measured at a constant swelling temperature of 25 °C. The width of the cotton linters without APS swelling was 14 ± 6 µm (Fig. 2a), which is in accordance with the FESEM image (Fig. S1). After swelling for 0.5 h, the width increased to 18 ± 5 µm (Fig. 2b). After swelling for 3.0 h, the width increased further to

27 ± 8 µm (Fig. 2c). After swelling for 6.0 h, the width was 29 ± 3 µm (Fig. 2d), which is not much different from that at 3.0 h, although there was evidence of more severe expansion at the ends, which is indicative of more oxidation.

Figure 3 shows the optical micrographs of the cotton linter samples at different temperatures. The widths of the linters at the swelling temperature of − 15 °C was 18 ± 8 µm (Fig. 3a). With the temperature increasing from − 15 to − 5 °C and then to 25 °C, the width increased to 22 ± 6 and 27 ± 8 µm, respectively (Fig. 3b). The sub-zero temperature freezes the solution, decreasing the fluidity and diffusivity of the liquid and weakening the swelling effect. Thus, a swelling temperature of 25 °C was chosen.

Structural analysis of the NCC suspension and particles

Figure 4 shows the XRD patterns of the cotton linter and NCC samples at different swelling temperatures, swelling times and S–L ratios. Both cotton linters and NCC samples have a sharp peak at $2\theta = 22.7°$ and two peaks at $2\theta = 14.7°$ and $16.7°$, corresponding to the cellulose crystal planes of (200) (1–10) and (110), respectively (Duchemin et al. 2009; Flauzino Neto et al. 2013). These are the characteristic diffraction peaks of cellulose I_β (Qi et al. 2009), indicating that the crystalline structure of cellulose did not change after the APS swelling and oxidation. The CI of all NCC samples was higher than that of the cotton linters (80.60%). As the swelling time increased, the highest crystallinity was obtained for the NCC (at 3.0 h). If the swelling time is too long, some of the APS is decomposed in the solution, resulting in a reduced amount of effective oxidative species for the desired oxidation reactions. As the swelling temperature increased, the CI of NCC also increased. At sub-zero temperatures, cotton linter may partially freeze, which has a negative effect on the diffusion of persulfate into the amorphous cellulose region. Therefore, a swelling temperature of 25 °C is optimal. When the S–L ratio was 1:50, the CI of NCC was at its maximum, indicating that the amorphous region of the cotton linter was destroyed most severely.

Figure 5 shows the FTIR spectra of cotton linter and NCC samples at different experimental conditions. The NCC infrared results were quite similar to
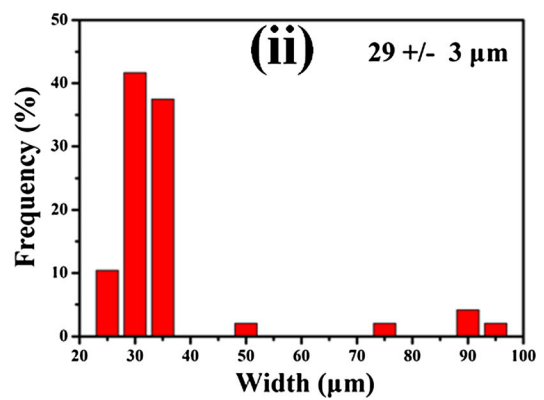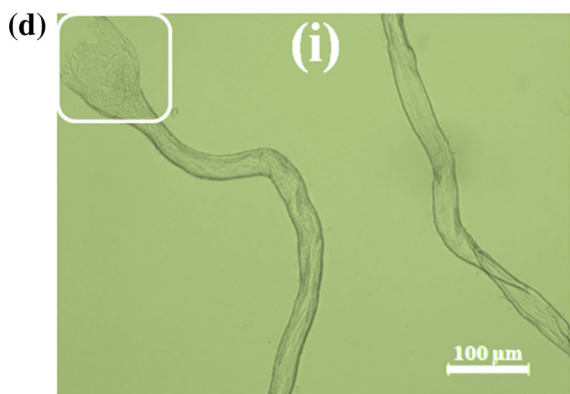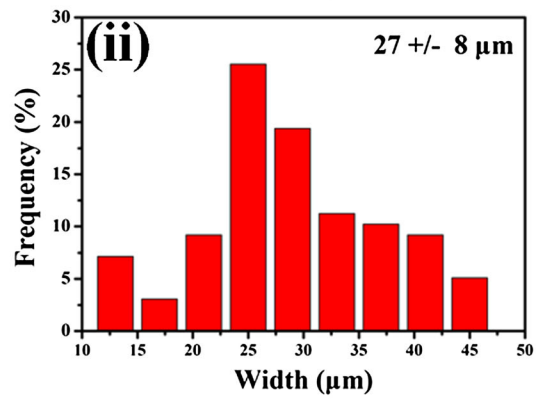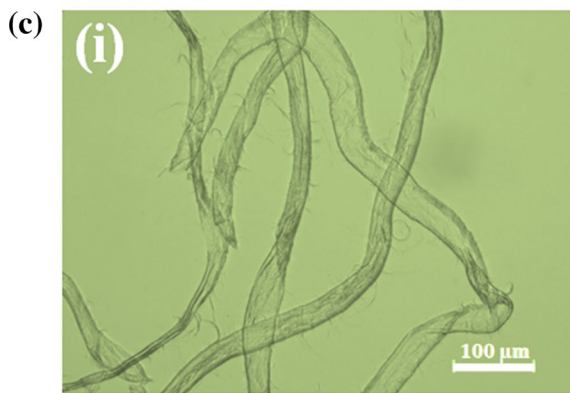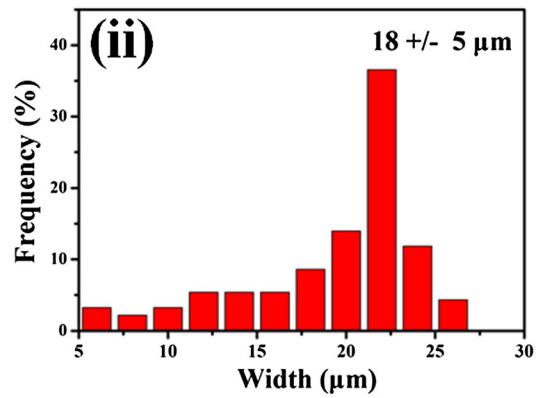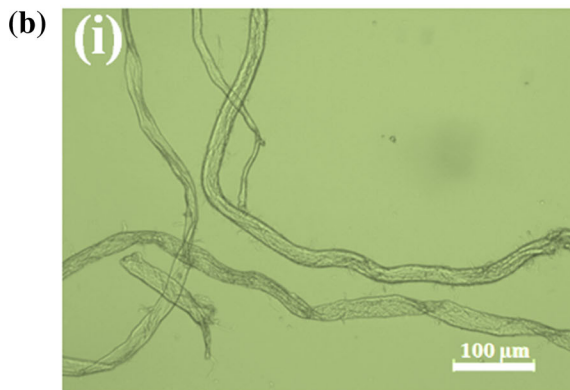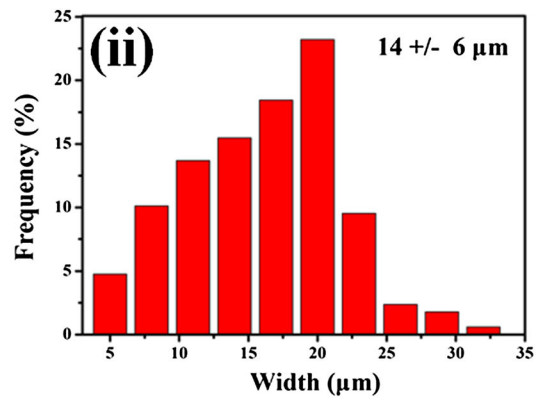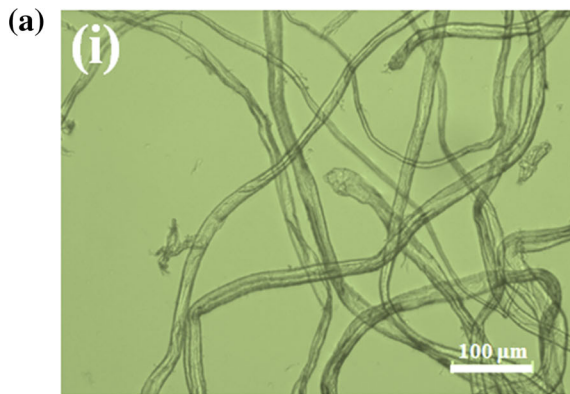
◀ **Fig. 2** Optical micrographs (i) and width distribution (ii) of the cotton linters at different swelling times of 0.0 h (**a**), 0.5 h (**b**), 3.0 h (**c**) and 6.0 h (**d**)

that of cotton linters, showing strong O–H stretching absorption (approximately 3340 cm^{-1}), –CH$_2$ stretching (approximately 2899 cm^{-1}), the carbonyl peak at C-6 (approximately 1734 cm^{-1}), the C–OH bending (approximately 1207 cm^{-1}), and the glycosidic bond,
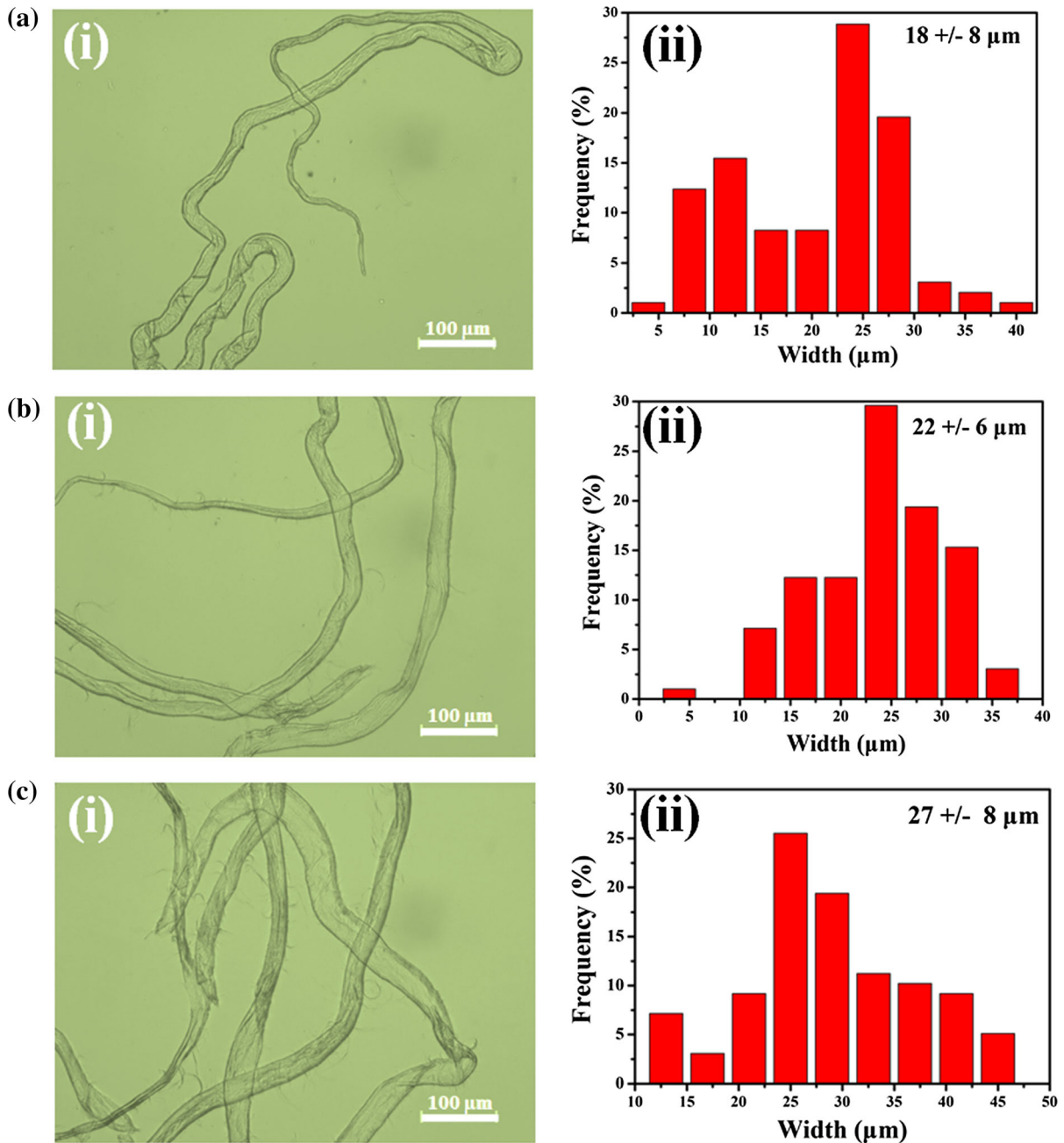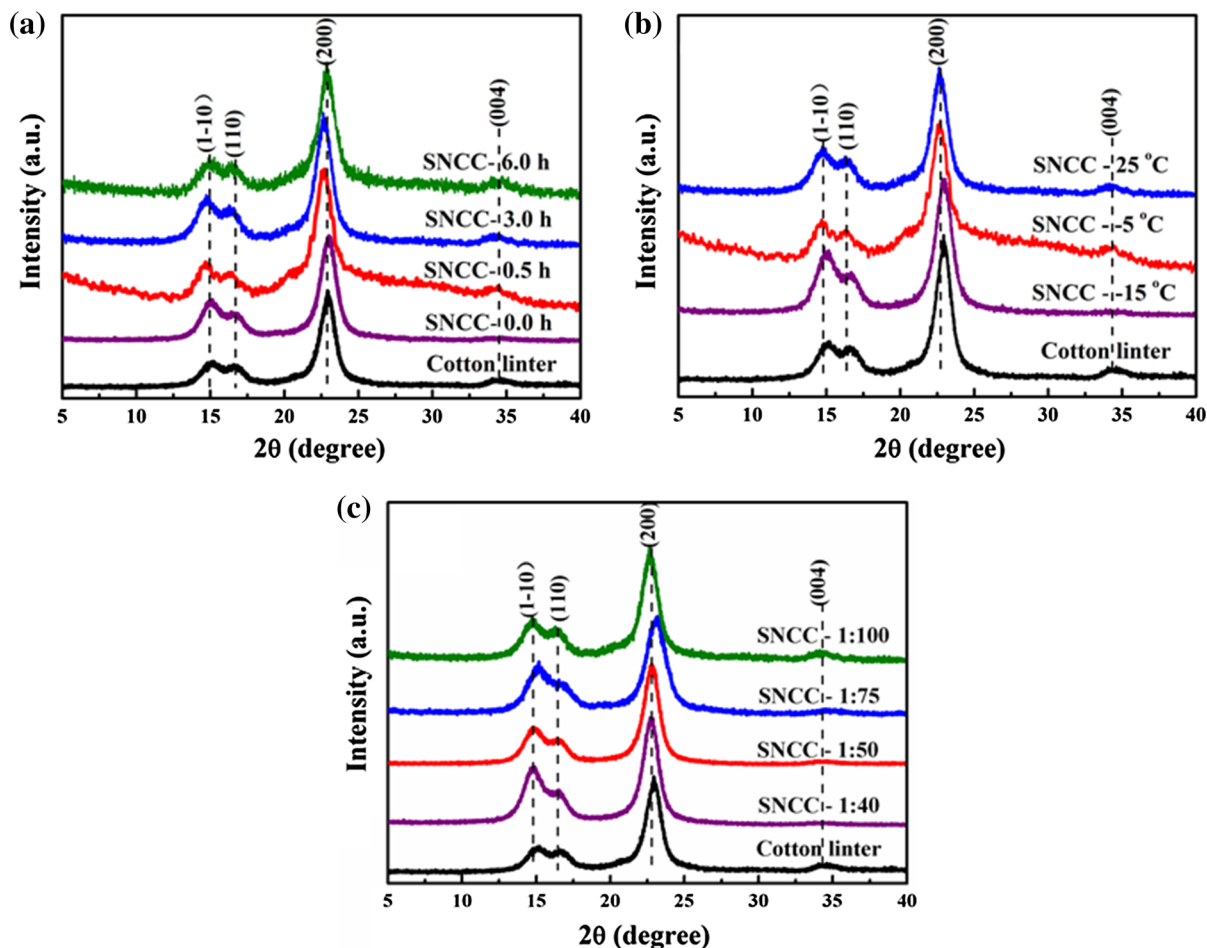

Fig. 3 Optical micrographs (i) and width distribution (ii) of the cotton linters at different swelling temperatures of − 15 °C (**a**), − 5 °C (**b**) and 25 °C (**c**)

Fig. 4 XRD patterns of the cotton linter and NCC samples obtained at different swelling times (**a**), swelling temperatures (**b**) and S–L ratios (**c**)

C–O–C stretching (approximately 1116 cm^{-1}). Compared with those of cotton linters, no apparent differences in the spectra of the NCC samples were obtained under different conditions, indicating that the NCC crystal structure did not change and the crystalline structure of cellulose I_β was maintained, which agree with the XRD patterns. However, for the NCC samples, the peak at 1207 cm^{-1} (C–OH bending (Han et al. 2013)) disappeared, and a new carbonyl peak at 1734 cm^{-1} (at C-6) appeared.

The peak area approximately 2899 cm^{-1} was selected as a benchmark to calculate the other peak areas of NCC. The results are shown in Table S1. The relative peak areas of S_{3340}/S_{2899}, S_{1739}/S_{2899} and S_{1112}/S_{2899} are indicative of the hydrogen bonding in NCC, the C–OH bond conversion to carboxyl at C-6 and the C–O–C bond of the glucose units,

respectively. The minimum peak area ratios of S_{3340}/S_{2899} and S_{1112}/S_{2899} and the maximum peak area of S_{1739}/S_{2899} were obtained at the optimum conditions of SNCC-3.0 h, SNCC-25 °C and SNCC-1:50. These results support the conclusion that the optimum conditions for preparing NCC from cotton linters are a swelling time of 3.0 h, a swelling temperature of 25 °C and an S–L ratio of 1:50.

Table 1 shows that the NCC yield of 94.91% was obtained at a swelling time of 3.0 h. As shown, with just direct heating and oxidation and no swelling, the NCC yield was low (64.24%). The swelling improves the accessibility of cotton linters towards oxidants (Hamad and Hu 2010). Moreover, a higher yield can be obtained at room temperature (25 °C) rather than at low temperatures. At an S–L ratio of 1:50, the maximum yield of 95.75% was obtained. It is also
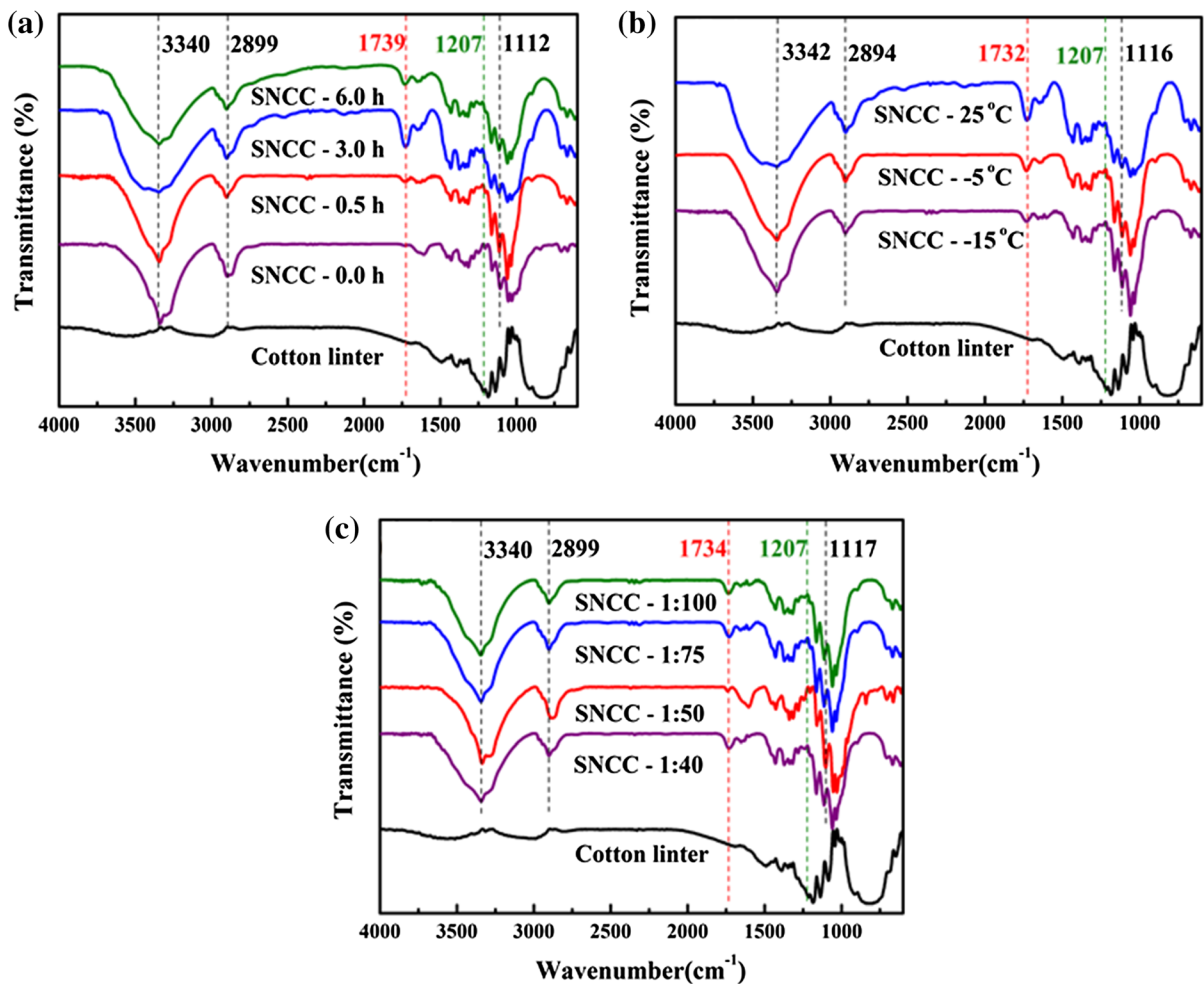
Fig. 5 FT-IR spectra of the cotton linters and NCC obtained at different swelling times (**a**), swelling temperatures (**b**) and S–L ratios (**c**)

clear that the increase in the S–L ratio from 1:50 to 1:100 does not have a significant role in the yield of NCC. Notably, the volume of the APS solution was reduced by half compared to the conventional methods.

As shown in Table 2, using the same raw cotton linters with different methods, the NCC yield of 95.75% prepared in this study at the optimal conditions was higher than that reported in other methods. The yield of NCC prepared by Shamskar et al. (2016) was 77.0% using H_2SO_4 hydrolysis, that prepared by Thambiraj and Shankaran (2017) was 91.0% via NaOH and H_2SO_4 hydrolysis, that prepared by Ling et al. (2019) and Liu et al. (2017) was 80–90% and 74.2% using DES treatment, respectively and that prepared by Montanari et al. (2005) was 81% via

TEMPO oxidation. Using the same source of cotton linters with the same method of APS oxidation, the optimal yield of NCC in our work was approximately 2.8 times higher than that prepared by Mascheroni et al. (2016) (34.4%). This finding indicates that APS swelling followed by oxidation is critical to reach the present result of a very high NCC yield.

Table 1 also shows the Zeta potential of NCC suspensions obtained from different preparation conditions. The Zeta potential of NCC suspensions ranged from − 30.5 to − 25.7 mV, which is due to the formation of carboxyl groups on the NCC surface as a result of APS oxidation. These carboxyl groups are responsible for the electrostatic repulsion between NCC particles, so they are stable in water (Pable et al. 2014; Yang et al. 2012; Yang and van de Ven

Table 1 Crystallinity index, Yield and Zeta potential of the cotton linter and NCC samples prepared at different swelling times, swelling temperatures and S–L ratios

Swelling time/h	Swelling temperature/°C	S–L ratio	CI/ %	Yield/%	DP	Zeta potential/mV
[a]_	–	–	80.60	–	764	–
0.0	25	1:100	85.12	64.24	291	− 25.7
0.5	25	1:100	86.93	72.34	271	− 27.5
3.0	25	1:100	90.91	94.91	157	− 29.9
6.0	25	1:100	81.26	89.15	276	− 28.9
3.0	− 15	1:100	81.22	91.84	246	− 29.4
3.0	− 5	1:100	83.31	90.22	237	− 29.2
3.0	25	1:100	90.91	94.91	157	− 29.9
3.0	25	1:40	83.23	81.59	213	− 28.5
3.0	25	1:50	93.51	95.75	139	− 30.5
3.0	25	1:75	85.70	90.51	212	− 29.3
3.0	25	1:100	90.91	94.91	157	− 29.9

[a]Cotton linters

Table 2 A comparison of the present work with previously reported methods without the swelling process using the same source

Source	Synthesis method	Morphology	Size/nm	Yield/%	References
Cotton	H$_2$SO$_4$ hydrolysis	Rod-like	25 (D[a]) 450 (L[b])	77.0	Shamskar et al. (2016)
Industrial waste cotton	NaOH and H$_2$SO$_4$ hydrolysis	Needle-like	10 ± 1 (D) 180 ± 60 (L)	91.0	Thambiraj and Shankaran (2017)
Cotton	TEMPO oxidation	Rod-like	4–5 (D)	81.0	Montanari et al. (2005)
Cotton	DES treatment	Needle-like	9–17 (D) 122.4–205.9 (average L)	80–90	Ling et al. (2019)
Cotton	DES treatment	Needle-like	3–25 (D) 100–350 (L)	74.2	Liu et al. (2017)
Cotton linters	APS oxidation	Rod-like	6.2 ± 0.9 (D) 121 ± 46 (L)	34.4	Mascheroni et al. (2016)
Cotton linters	APS swelling and oxidation	Spindle-like	10 ± 5 (D) 136 ± 90 (L)	95.75	This work

[a]The diameter of NCC

[b]The length of NCC

2016). As shown in Fig. S2, the NCC suspension with a concentration of 1.0 wt% is observed to be transparent, stable and uniformly dispersed.

The average DP values of the cotton linters and NCC samples were studied and listed in Table 1. The DP value of cotton linters exhibited a significant decrease from 764 to 291, 271, 157, 276, 246, 237, 213, 139 and 181 in the different experimental conditions after APS swelling followed by oxidation. This suggests that the molecular chains of cellulose were fragmented in the amorphous region at certain intervals, as reported by Sun et al. (2016).

AFM and height profile images of the NCC samples prepared at different conditions and their diameter and

length distribution, aspect ratio and Ra are presented in Figs. 6, 7 and 8 and Table S2. The NCC particles possess a spindle-like shape with length distributions of 174 ± 109, 177 ± 105, 136 ± 88, and 179 ± 100 nm and diameter distributions of 10 ± 5, 23 ± 9, 12 ± 5 and 26 ± 12 nm for swelling times of 0.0, 0.5, 3.0 and 6.0 h, respectively (Fig. 6). The

length and diameter of the NCC were the lowest for a swelling time of 3.0 h. The average length and diameter of the NCC particles increased with the increase of swelling time to 6.0 h. The NCC particles possess a spindle-like shape with length distributions of 193 ± 115, 166 ± 85, and 136 ± 88 nm and diameter distributions of 17 ± 6, 14 ± 6 and
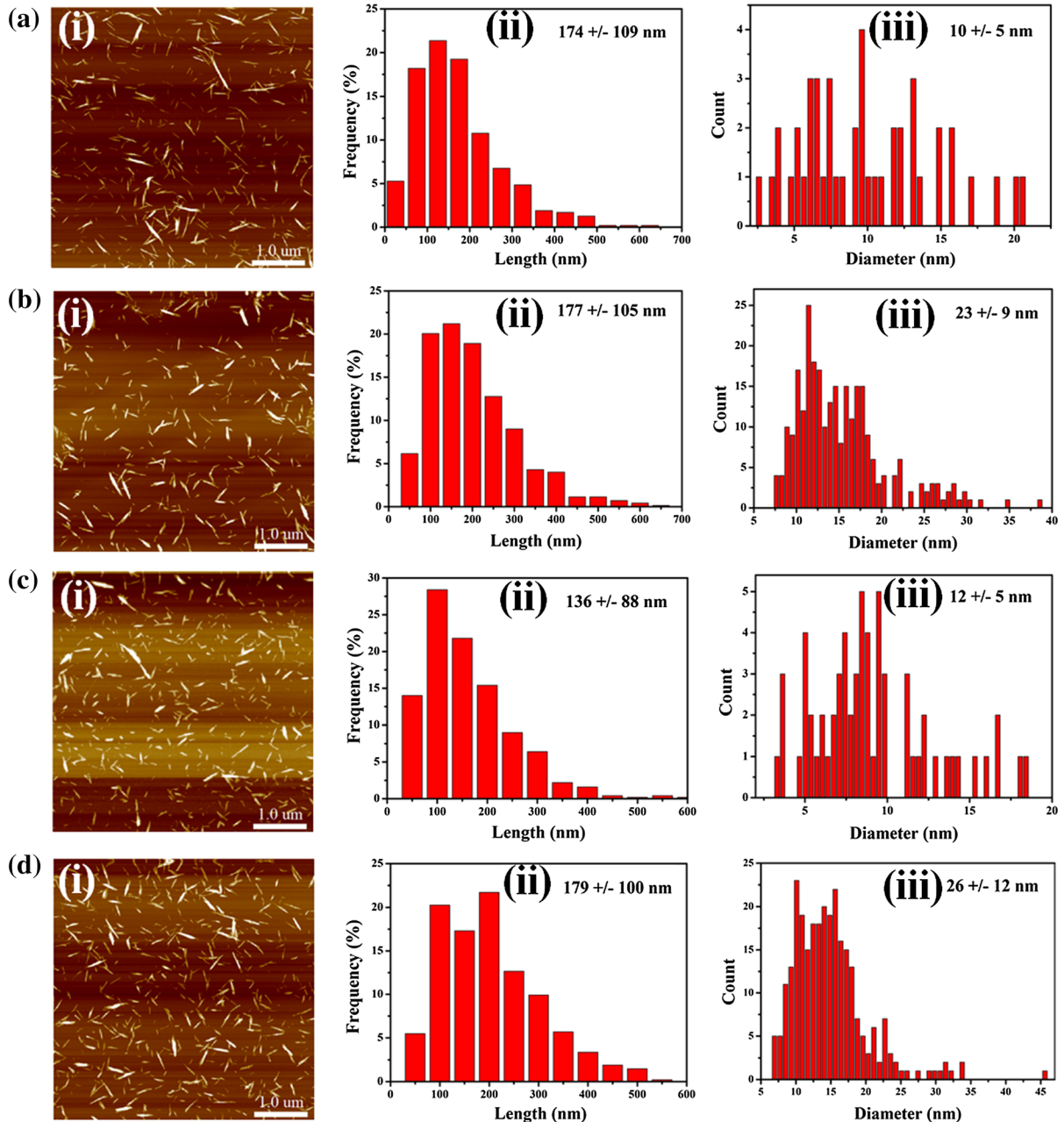

Fig. 6 AFM images (i), length (ii) and diameter (iii) distribution of NCC samples obtained at different swelling times of 0.0 h (**a**), 0.5 h (**b**), 3.0 h (**c**) and 6.0 h (d)
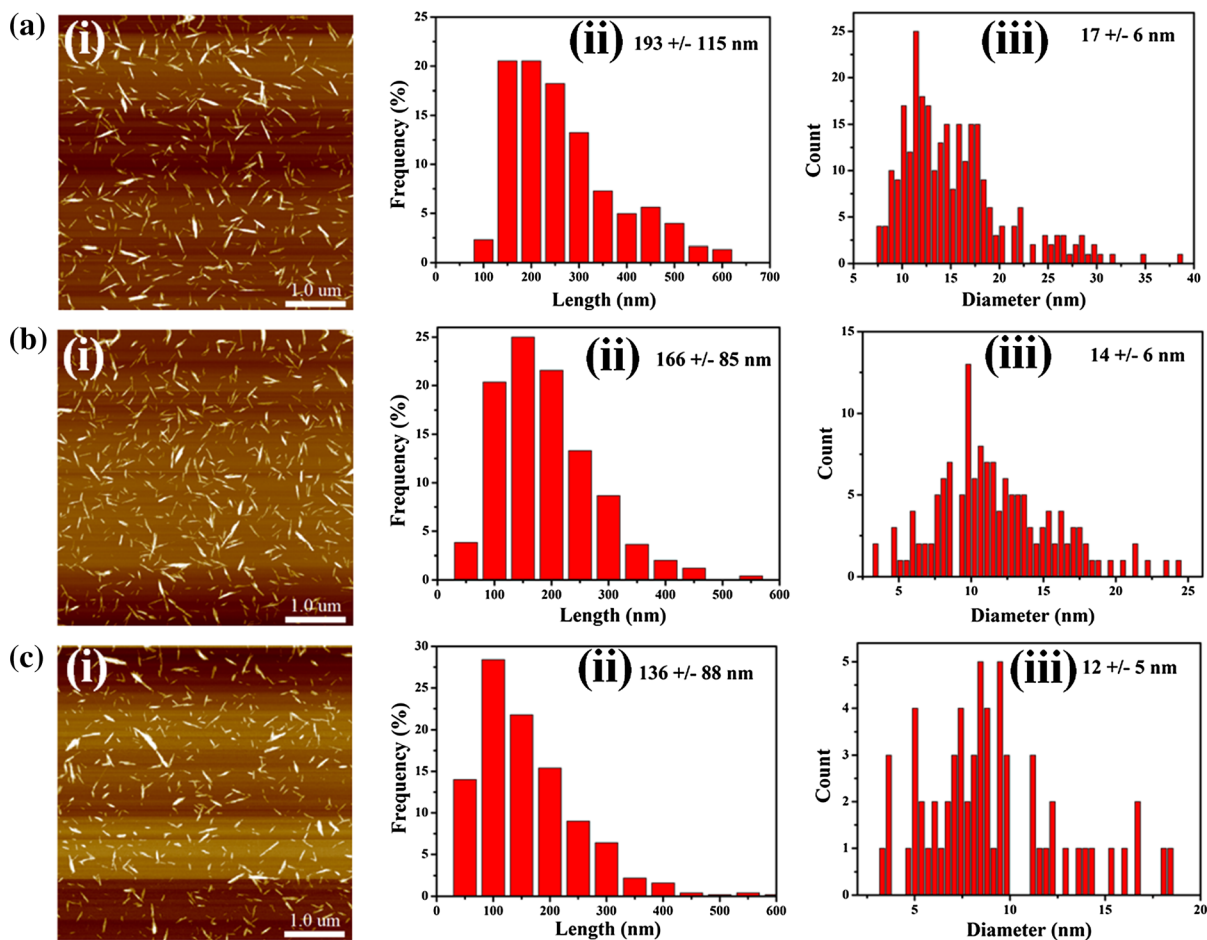
Fig. 7 - AFM images (i), length (ii) and diameter (iii) distribution of NCC samples obtained at different swelling temperatures of − 15 °C (**a**), − 5 °C (**b**) and 25 °C (**c**)

12 ± 5 nm for swelling temperatures of − 15 °C, − 5 °C and 25 °C, respectively (Fig. 7). The best swelling occurred at room temperature, which was conductive to minimize the decomposition of APS. The spindle shaped NCC particles with length distributions of 192 ± 101, 136 ± 90, 184 ± 100, and 136 ± 88 nm and diameter distributions of 17 ± 6, 10 ± 5, 11 ± 3 and 12 ± 5 nm were observed in the samples prepared with S–L ratios of 1:40, 1:50, 1:75 and 1:100, respectively (Fig. 8). Thus, it is evident that at an S–L ratio of 1:50, the length of the NCC particles is 136 ± 90 nm, which is almost the same as that obtained at the optimal swelling time (3.0 h) and optimal temperature (25 °C). Its diameter was 10 ± 5 nm, resulting in a high aspect ratio. The results on the aspect ratio ranged from 1 to 100 as shown in Table S3, which plays an important role in

the formation of layer-by-layer self-assembly of NCC layers after natural evaporation (Han et al. 2013).

In the height profile images, the curves of single NCC are jagged with different widths and heights (Figs. S3–S5). At the same time, the "linear" micro roughness (Ra) of NCC ranges from 1.9 to 2.4 nm (Table S3). These two analyses strongly validate that the surface of single NCC is not smooth and contains some gullies. The high-resolution AFM 3D image of NCC shows that the surfaces have peaks and valleys, indicating that the individual NCC may have helical structures (Fig. S6), consistent with the height profile curves and Ra.

The TGA and DTG results of the cotton linters and NCC samples obtained under different conditions are shown in Fig. 9 and Fig. S7. The main weight loss of the cotton linters is related to cellulose degradation,
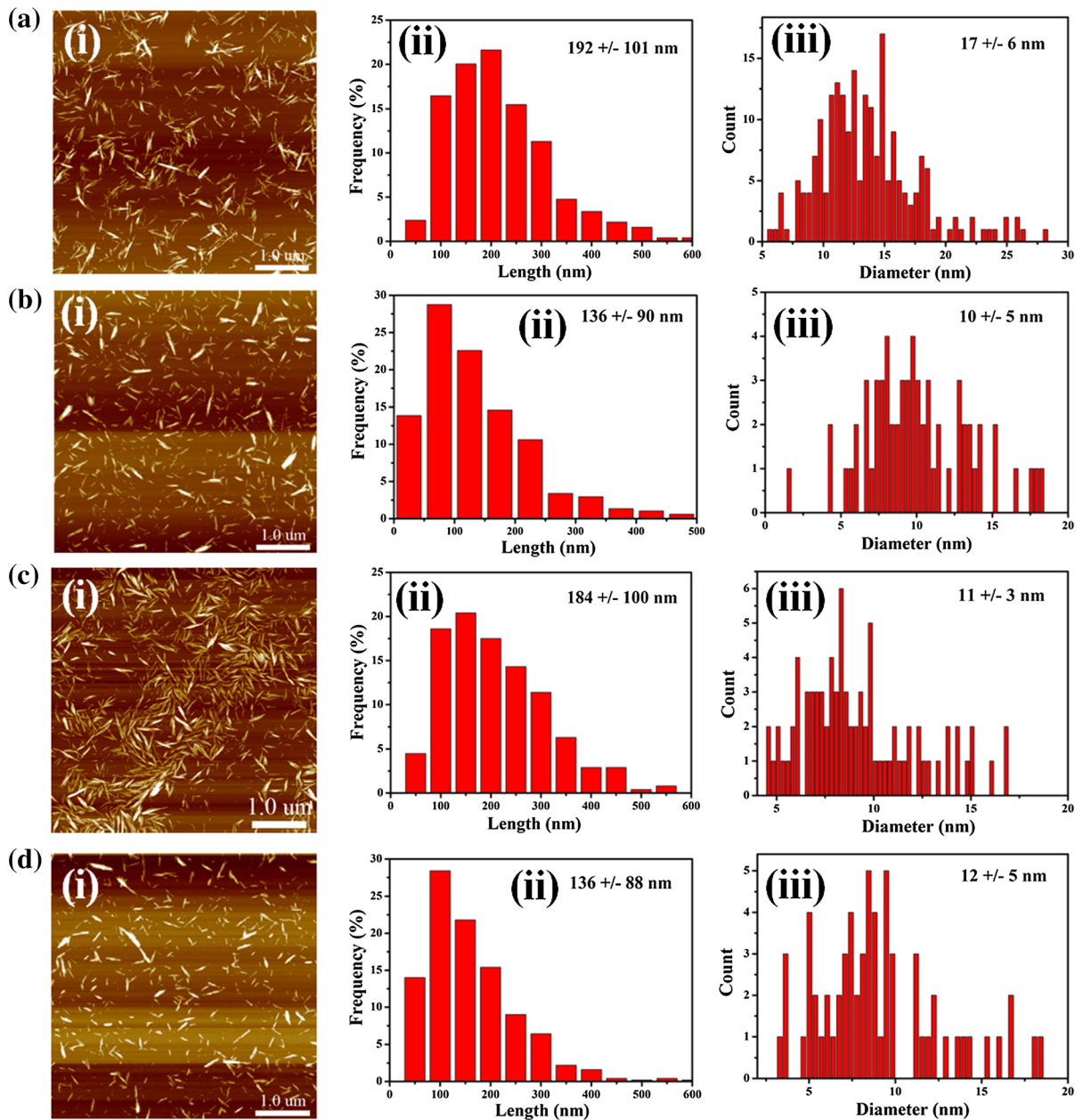
Fig. 8 AFM images (i), length (ii) and diameter (iii) distribution of NCC samples obtained at different S–L ratios of 1:40 (**a**), 1:50 (**b**), 1:75 (**c**) and 1:100 (**d**)

which occurs in the range of 322–378 °C (Sonia and Priya Dasan 2013) (Fig. 9a). The NCC samples obtained at different conditions exhibited gradual weight loss in the range of 210–378 °C (Fig. 9b–d). As shown in Table 3, the onset degradation temperatures of cotton linters, SNCC-3.0 h, SNCC-25 °C

and SNCC-1:50 are 322 °C, 226 °C, 226 °C and 219 °C, respectively, whereas the decomposition temperatures are 361 °C, 333 °C, 333 °C and 360 °C, respectively. Compared to cotton linters, the rate and weight loss of NCC was much lower. These results illustrate that the thermal stability of NCC
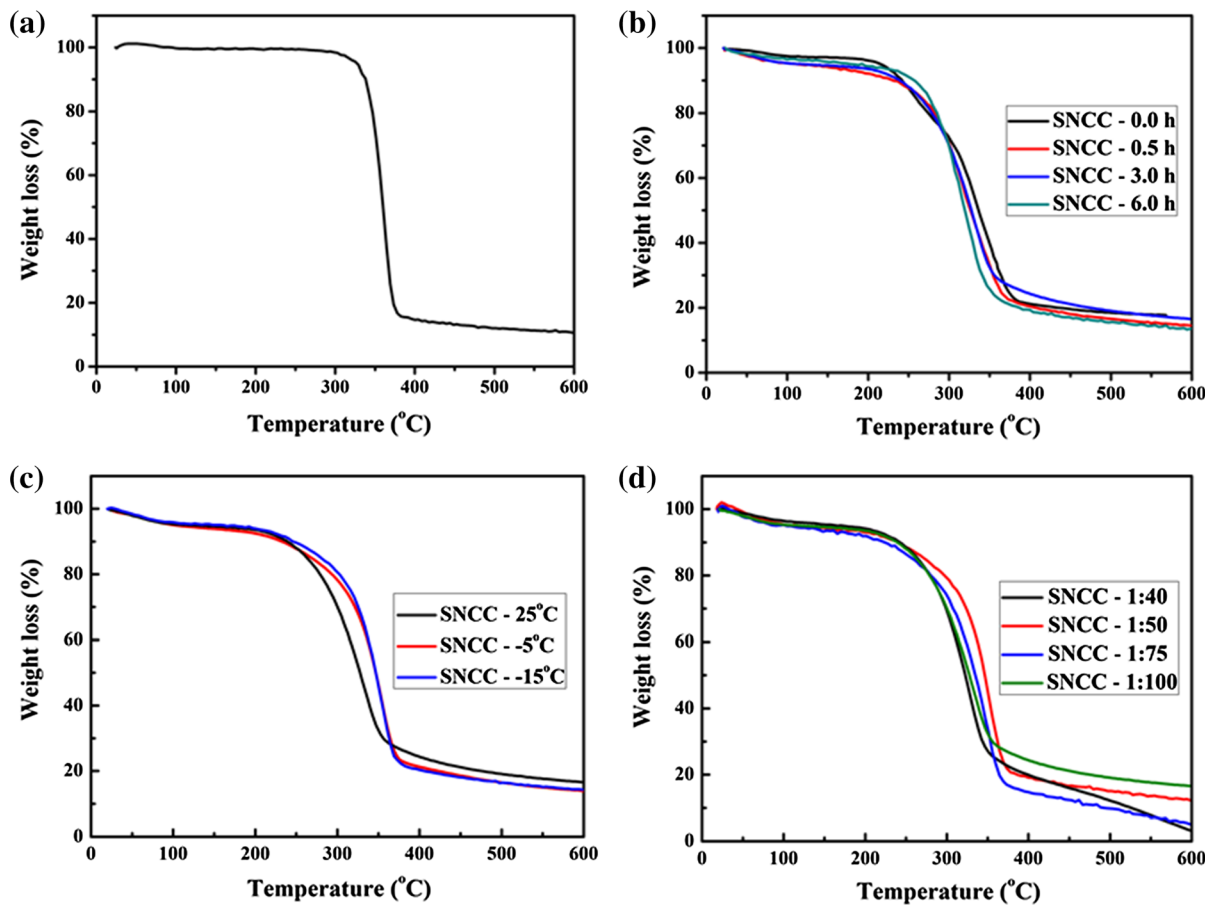
Fig. 9 TGA curves of the cotton linters (**a**) and NCC at different swelling times (**b**), swelling temperatures (**c**) and solid–liquid ratios (**d**)

Table 3 The thermogravimetric analyses of cotton linters and NCC samples obtained at different swelling times, swelling temperatures and S–L ratios

Swelling time/h	Swelling temperature/°C	S–L ratio	T_{onset}/°C	T_{peak}/°C	W_{loss}/%
[a]_	–	–	322	361	83.62
0.0	25	1:100	215	333	77.50
0.5	25	1:100	240	318	76.37
3.0	25	1:100	226	333	72.86
6.0	25	1:100	231	325	76.05
3.0	− 15	1:100	245	354	75.26
3.0	− 5	1:100	233	355	71.68
3.0	25	1:100	226	333	72.86
3.0	25	1:40	226	333	73.22
3.0	25	1:50	219	360	77.45
3.0	25	1:75	240	343	82.94
3.0	25	1:100	226	333	72.86

[a]Cotton linters

Fig. 10 POM images of the NCC suspension during evaporation (**a**) and after drying (film) (**b**); FESEM micrographs of the cross-section of film (**c**–**e**) at a swelling time of 3.0 h, swelling temperature of 25 °C and S–L ratio of 1:50; Schematic representation of the NCC chiral self-assembly structure (**f**); FESEM micrographs of the cross-section of film (**g**, **h**) at a swelling time of 3.0 h, swelling temperature of 25 °C and S–L ratio of 1:100
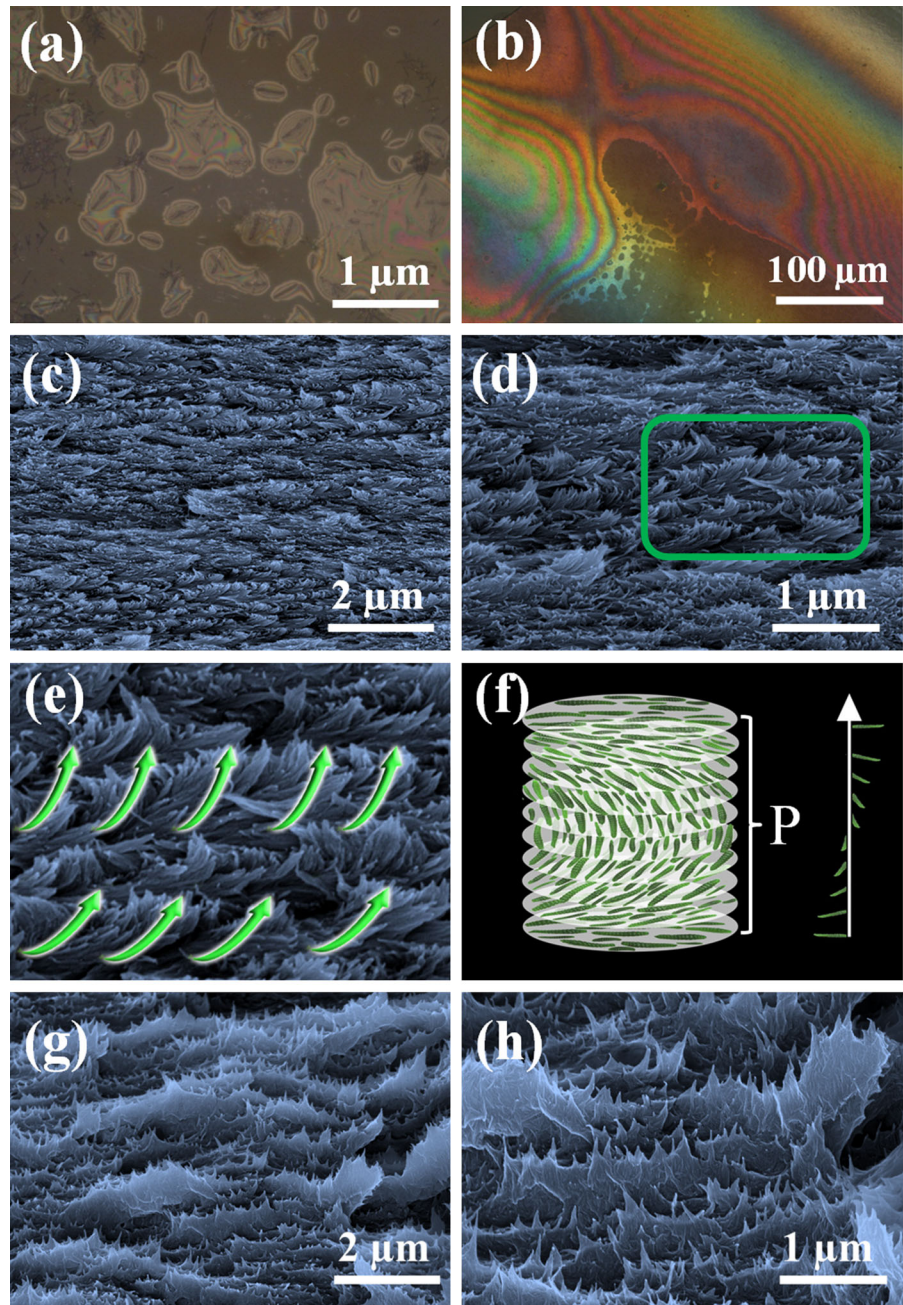
samples is significantly increased compared to that of cotton linters (Shankar and Rhim 2016). Amongst the different samples, the sample prepared at a swelling temperature of 25 °C and S–L ratio of 1:50 displayed better thermal stability and lower weight loss.

Based on the results of the swelling followed by oxidation, the optimum conditions for NCC synthesis were a swelling time of 3.0 h, a swelling temperature of 25 °C and an S–L ratio of 1:50. A possible mechanism is then illustrated as follows. The H_2O molecules carrying the $S_2O_8^{2-}$ ions play a major

role in the process of swelling by diffusing into the amorphous region of cellulose fibre (Mantanis et al. 1995; Pei et al. 2019; Spinu et al. 2011; Zhang et al. 2006) and laying the foundation for the next step of oxidation. Upon heating at 60 °C, the persulfate enters into the amorphous region of cellulose and produces active $SO_4\cdot^-$ and H_2O_2, which effectively attack the two-phase structure of cellulose and oxidize the –OH group at the C-6 position. The swelling temperature of 25 °C plays an effectively crucial role in breaking the hydrogen bonds between the molecular chains of cellulose. It permits the preparation of NCC with a high yield and crystallinity index. $SO_4\cdot^-$ and H_2O_2 have strong oxidizability and low molecular weights; thus, they can easily oxidize the reducible groups in the amorphous region and break the intra and inter-molecular hydrogen bonds (Lam et al. 2012; Moon et al. 2011).

Chiral self-assembly of the NCC film

The NCC sample prepared at the optimum conditions such as a swelling time of 3.0 h, a swelling temperature of 25 °C and an S–L ratio of 1:50 and the sample prepared with the S–L ratio of 1:100 was used for the preparation of NCC films. The NCC suspension was naturally evaporated with the eventual formation of a transparent and brittle film (Fig. 1). Due to its brittleness, its application is very limited. Therefore, several methods have been reported to solve this issue. It can be solved by the addition of some water soluble polymers such as sodium poly acrylate and poly(ethylene glycol) (Bardet et al. 2015), poly(vinyl alcohol) and styrene butadiene (Zou et al. 2016) or cellulose nanofibrils (Xiong et al. 2014) to produce flexible and birefringent composites (Guidetti et al. 2016). The increased CI of the as-prepared NCC was expected to increase the stiffness and rigidity (Islam et al. 2018). The POM images of the film exhibited the appearance of iridescence in the drying process (Fig. 10a, b), supporting the conclusion that the as-prepared NCC particles are spiral and chiral (Revol et al. 1992; Sharma et al. 2009). The chiral nematic phase of NCC films was further demonstrated by FESEM micrographs. A layer-by-layer structure on its cross-section (Fig. 10c, g) is clearly evident due to the change of the direction of the helical axis of the chiral nematic phase, as reported previously (Majoinen et al. 2012; Straley 1976). In the SEM images, the helical

pitch distance was observed to be in the order of several hundred nanometres in between each layer (Fig. 10d, h) that were arranged in a counter-clockwise pattern (a left-hand pattern, Fig. 10e). A schematic representation of the NCC chiral self-assembly structure is shown in Fig. 10f.

Conclusion

This study focused on the development of a green and sustainable method for preparing NCC from cotton linters, which is based on ammonium persulfate assisted swelling followed by oxidation. The reaction parameters for preparing NCC were investigated in detail. The optimum conditions were as follows: a swelling time of 3.0 h, a swelling temperature of 25 °C and an S–L ratio of 1:50. The NCC suspension is a transparent liquid with uniform dispersion while no NCC agglomeration is observed. The NCC yield, crystallinity index and Zeta potential under optimized conditions were 95.75%, 83.51%, and − 30.5 mV, respectively. The length, diameter, aspect ratio and roughness of the NCC particles with a spindle-shaped helical structure were 136 ± 90 nm, 10 ± 5 nm, 3.1–45.2 and 2.2 nm, respectively. Moreover, the swelling plays a crucial role in the preparation of NCC by the APS oxidation method, which shortens the reaction time, decreases the APS volume and improves the NCC yield, while simultaneously decreasing the particle size. The FESEM and POM micrographs exhibited a layered structure perpendicular to the surface and iridescence of transparent films with a fingerprint texture. A chiral nematic phase is formed during drying.

Compliance with ethical standards

Conflict of interest The authors declare that they have no conflict of interest.

References

Abitbol T, Kloser E, Gray DG (2013) Estimation of the surface sulfur content of cellulose nanocrystals prepared by sulfuric acid hydrolysis. Cellulose 20:785–794

Asefa T (2012) Chiral nematic mesoporous carbons from self-assembled nanocrystalline cellulose. Angew Chem Int Ed 51:2008–2010

Bardet R, Belgacem N, Bras J (2015) Flexibility and color monitoring of cellulose nanocrystal iridescent solid films using anionic or neutral polymers. ACS Appl Mater Interfaces 7:4010–4018

Batmaz R, Mohammed N, Zaman M, Minhas G, Berry RM, Tam KC (2014) Cellulose nanocrystals as promising adsorbents for the removal of cationic dyes. Cellulose 21:1655–1665

Carlsson DO, Lindh J, Nyholm L, Strømme M, Mihranyan A (2014) Cooxidant-free TEMPO-mediated oxidation of highly crystalline nanocellulose in water. RSC Adv 4:52289–52298

Castro-Guerrero CF, Gray DG (2014) Chiral nematic phase formation by aqueous suspensions of cellulose nanocrystals prepared by oxidation with ammonium persulfate. Cellulose 21:2567–2577

Cellulose In: Ullmann's Encyclopedia of Industrial Chemistry

Chen W, Li Q, Cao J, Liu Y, Li J, Zhang J, Luo S, Yu H (2015) Revealing the structures of cellulose nanofiber bundles obtained by mechanical nanofibrillation via TEM observation. Carbohydr Polym 117:950–956

Cheng M, Qin Z, Liu Y, Qin Y, Li T, Chen L, Zhu M (2014) Efficient extraction of carboxylated spherical cellulose nanocrystals with narrow distribution through hydrolysis of lyocell fibers by using ammonium persulfate as an oxidant. J Mater Chem A 2:251–258

Cheng S, Zhang Y, Cha R, Yang J, Jiang X (2016) Water-soluble nanocrystalline cellulose films with highly transparent and oxygen barrier properties. Nanoscale 8:973–978

Chindawong C, Johannsmann D (2014) An anisotropic ink based on crystalline nanocellulose: potential applications in security printing. J Appl Polym Sci 131(22):41063

Cui S, Zhang S, Ge S, Xiong L, Sun Q (2016) Green preparation and characterization of size-controlled nanocrystalline cellulose via ultrasonic-assisted enzymatic hydrolysis. Ind Crops Prod 83:346–352

Cuissinat C, Navard P (2006) Swelling and dissolution of cellulose part II: free floating cotton and wood fibres in NaOH–water–additives systems. Macromol Symp 244:19–30

Domingues RMA, Gomes ME, Reis RL (2014) The potential of cellulose nanocrystals in tissue engineering strategies. Biomacromol 15(7):2327–2346

Dong S, Roman M (2007) Fluorescently labeled cellulose nanocrystals for bioimaging applications. J Am Chem Soc 129:13810–13811

Duchemin BJC, Mathew AP, Oksman K (2009) All-cellulose composites by partial dissolution in the ionic liquid 1-butyl-3-methylimidazolium chloride. Compos A Appl Sci Manuf 40:2031–2037

Fang Z, Zhu H, Yuan Y, Ha D, Zhu S, Preston C, Chen Q, Li Y, Han X, Lee S, Chen G, Li T, Munday J, Huang J, Hu L (2014) Novel nanostructured paper with ultrahigh transparency and ultrahigh haze for solar cells. Nano Lett 14(2):765–773

Flauzino Neto WP, Silvério HA, Dantas NO, Pasquini D (2013) Extraction and characterization of cellulose nanocrystals from agro-industrial residue—Soy hulls. Ind Crops Prod 42:480–488

Gardner KH, Blackwell J (1974) The structure of native cellulose. Biopolymers 13:1975–2001

Guidetti G, Atifi S, Vignolini S, Hamad WY (2016) Flexible photonic cellulose nanocrystal films. Adv Mater 28:10042–10047

Hamad WY, Hu TQ (2010) Structure–process–yield interrelations in nanocrystalline cellulose extraction. Can J Chem Eng 88:392–402

Han J, Zhou C, Wu Y, Liu F, Wu Q (2013) Self-assembling behavior of cellulose nanoparticles during freeze-drying: effect of suspension concentration, particle size, crystal structure, and surface charge. Biomacromol 14:1529–1540

Huang J, Zhu H, Chen Y, Preston C, Rohrbach K, Cumings J, Hu L (2013) Highly Transparent and Flexible Nanopaper Transistors. ACS Nano 7(3):2106–2113

Huq T, Salmieri S, Khan A, Khan RA, Le Tien C, Riedl B, Fraschini C, Bouchard J, Uribe-Calderon J, Kamal MR, Lacroix M (2012) Nanocrystalline cellulose (NCC) reinforced alginate based biodegradable nanocomposite film. Carbohydr Polym 90:1757–1763

Immergut E, Ranby B, Mark H (1953) Recent work on molecular weight of cellulose. Ind Eng Chem 45:2483–2490

Islam MS, Kao N, Bhattacharya SN, Gupta R, Choi HJ (2018) Potential aspect of rice husk biomass in Australia for nanocrystalline cellulose production. Chin J Chem Eng 26:465–476

Isogai A, Saito T, Fukuzumi H (2011) TEMPO-oxidized cellulose nanofibers. Nanoscale 3:71–85

Jackson JK, Letchford K, Wasserman BZ, Ye L, Hamad WY, Burt HM (2011) The use of nanocrystalline cellulose for the binding and controlled release of drugs. Int J Nanomed 6:321–330

Kian LK, Jawaid M, Ariffin H, Karim Z (2018) Isolation and characterization of nanocrystalline cellulose from roselle-derived microcrystalline cellulose. Int J Biol Macromol 114:54–63

Klemm D, Heublein B, Fink H-P, Bohn A (2005) Cellulose: fascinating Biopolymer and Sustainable Raw Material. Angew Chem Int Ed 44:3358–3393

Lam E, Hrapovic S, Majid E, Chong JH, Luong JHT (2012) Catalysis using gold nanoparticles decorated on nanocrystalline cellulose. Nanoscale 4:997–1002

Lee M, Heo MH, Lee H, Lee H-H, Jeong H, Kim Y-W, Shin J (2018) Facile and eco-friendly extraction of cellulose nanocrystals via electron beam irradiation followed by high-pressure homogenization. Green Chem 20:2596–2610

Leung ACW, Hrapovic S, Lam E, Liu Y, Male KB, Mahmoud KA, Luong JHT (2011) Characteristics and properties of carboxylated cellulose nanocrystals prepared from a novel one-step procedure. Small 7:302–305

Lin N, Bruzzese C, Dufresne A (2012) TEMPO-oxidized nanocellulose participating as crosslinking aid for alginate-based sponges. ACS Appl Mater Interfaces 4:4948–4959

Ling Z, Edwards JV, Guo Z, Prevost NT, Nam S, Wu Q, French AD, Xu F (2019) Structural variations of cotton cellulose nanocrystals from deep eutectic solvent treatment: micro and nano scale. Cellulose 26:861–876

Liu Y, Wang Q (2014) Removal of elemental mercury from flue gas by thermally activated ammonium persulfate in a bubble column reactor. Environ Sci Technol 48:12181–12189

Liu Y, Guo B, Xia Q, Meng J, Chen W, Liu S, Wang Q, Liu Y, Li J, Yu H (2017) Efficient cleavage of strong hydrogen bonds in cotton by deep eutectic solvents and facile fabrication of cellulose nanocrystals in high yields. ACS Sustain Chem Eng 5:7623–7631

Lu Q, Cai Z, Lin F, Tang L, Wang S, Huang B (2016a) Extraction of cellulose nanocrystals with a high yield of 88% by simultaneous mechanochemical activation and phosphotungstic acid hydrolysis. ACS Sustain Chem Eng 4:2165–2172

Lu Q, Cai Z, Lin F, Tang L, Wang S, Huang B (2016b) Extraction of cellulose nanocrystals with a high yield of 88% by simultaneous mechanochemical activation and phosphotungstic acid hydrolysis. ACS Sustain Chem Eng 4(4):2165–2172

Ma Y, Xia Q, Liu Y, Chen W, Liu S, Wang Q, Liu Y, Li J, Yu H (2019) Production of nanocellulose using hydrated deep eutectic solvent combined with ultrasonic treatment. ACS Omega 4:8539–8547

Mahmoud KA, Male KB, Hrapovic S, Luong JHT (2009) Cellulose nanocrystal/gold nanoparticle composite as a matrix for enzyme immobilization. ACS Appl Mater Interfaces 1:1383–1386

Majoinen J, Kontturi E, Ikkala O, Gray DG (2012) SEM imaging of chiral nematic films cast from cellulose nanocrystal suspensions. Cellulose 19:1599–1605

Mantanis GI, Young RA, Rowell RM (1994) Swelling of wood. Wood Sci Technol 28:119–134

Mantanis GI, Young RA, Rowell RM (1995) Swelling of compressed cellulose fiber webs in organic liquids. Cellulose 2:1–22

Mascheroni E, Rampazzo R, Ortenzi MA, Piva G, Bonetti S, Piergiovanni L (2016) Comparison of cellulose nanocrystals obtained by sulfuric acid hydrolysis and ammonium persulfate, to be used as coating on flexible food-packaging materials. Cellulose 23:779–793

Mohanta V, Madras G, Patil S (2014) Layer-by-layer assembled thin films and microcapsules of nanocrystalline cellulose for hydrophobic drug delivery. ACS Appl Mater Interfaces 6:20093–20101

Montanari S, Roumani M, Heux L, Vignon MR (2005) Topochemistry of carboxylated cellulose nanocrystals resulting from TEMPO-mediated oxidation. Macromolecules 38:1665–1671

Moon RJ, Martini A, Nairn J, Simonsen J, Youngblood J (2011) Cellulose nanomaterials review: structure, properties and nanocomposites. Chem Soc Rev 40:3941–3994

Ooi SY, Ahmad I, Amin MCIM (2016) Cellulose nanocrystals extracted from rice husks as a reinforcing material in gelatin hydrogels for use in controlled drug delivery systems. Ind Crops Prod 93:227–234

Pable D, Chattergi S, Venugopalan MV, Sen TK, Giri JD, Sarkar D (2014) Soil quality assessment using fuzzy modelling - a case study in rainfed cotton growing agro-ecological sub-regions of vidarbha, Maharashtra Cotton Res J 5(2):126–131

Pei L, Luo Y, Gu X, Dou H, Wang J (2019) Diffusion mechanism of aqueous solutions and swelling of cellulosic fibers in silicone non-aqueous dyeing system. Polymers 11:411

Potthast A, Rosenau T, Kosma P (2006) Analysis of oxidized functionalities in cellulose. In: Klemm D (ed) Polysaccharides II. Springer, Berlin, pp 1–48

Qi H, Cai J, Zhang L, Kuga S (2009) Properties of films composed of cellulose nanowhiskers and a cellulose matrix regenerated from alkali/urea solution. Biomacromol 10:1597–1602

Revol JF, Bradford H, Giasson J, Marchessault RH, Gray DG (1992) Helicoidal self-ordering of cellulose microfibrils in aqueous suspension. Int J Biol Macromol 14:170–172

Röder T, Morgenstern B, Schelosky N, Glatter O (2001) Solutions of cellulose in N,N-dimethylacetamide/lithium chloride studied by light scattering methods. Polymer 42:6765–6773

Saito T, Isogai A (2004) TEMPO-mediated oxidation of native cellulose. the effect of oxidation conditions on chemical and crystal structures of the water-insoluble fractions. Biomacromol 5:1983–1989

Schneider M, Graillat C, Boutti S, McKenna TF (2001) Decomposition of APS and H2O2 for emulsion polymerisation. Polym Bull 47:269–275

Segal L, Creely JJ, Martin AE, Conrad CM (1959) An empirical method for estimating the degree of crystallinity of native cellulose using the x-ray diffractometer. Text Res J 29:786–794

Shamskar KR, Heidari H, Rashidi A (2016) Preparation and evaluation of nanocrystalline cellulose aerogels from raw cotton and cotton stalk. Ind Crops Prod 93:203–211

Shankar S, Rhim J-W (2016) Preparation of nanocellulose from micro-crystalline cellulose: the effect on the performance and properties of agar-based composite films. Carbohydr Polym 135:18–26

Sharma V, Crne M, Park JO, Srinivasarao M (2009) Structural origin of circularly polarized iridescence in jeweled beetles. Science 325:449

Shopsowitz KE, Qi H, Hamad WY, MacLachlan MJ (2010) Free-standing mesoporous silica films with tunable chiral nematic structures. Nature 468:422

Sirviö JA, Visanko M, Liimatainen H (2016) Acidic deep eutectic solvents as hydrolytic media for cellulose nanocrystal production. Biomacromol 17:3025–3032

Sonia A, Priya Dasan K (2013) Chemical, morphology and thermal evaluation of cellulose microfibers obtained from Hibiscus sabdariffa. Carbohydr Polym 92:668–674

Spinu M, Dos Santos N, Le Moigne N, Navard P (2011) How does the never-dried state influence the swelling and dissolution of cellulose fibres in aqueous solvent? Cellulose 18:247–256

Straley JP (1976) Theory of piezoelectricity in nematic liquid crystals, and of the cholesteric ordering. Phys Rev A 14:1835–1841

Sun B, Zhang M, Hou Q, Liu R, Wu T, Si C (2016) Further characterization of cellulose nanocrystal (CNC) preparation from sulfuric acid hydrolysis of cotton fibers. Cellulose 23:439–450

Thambiraj S, Shankaran DR (2017) Preparation and physico-chemical characterization of cellulose nanocrystals from industrial waste cotton. Appl Surf Sci 412:405–416

Wang Z, Wang Z, Ye Y, Chen N, Li H (2016) Study on the removal of nitric oxide (NO) by dual oxidant (H2O2/S2O82 −) system. Chem Eng Sci 145:133–140

Xiong R, Han Y, Wang Y, Zhang W, Zhang X, Lu C (2014) Flexible, highly transparent and iridescent all-cellulose hybrid nanopaper with enhanced mechanical strength and writable surface. Carbohydr Polym 113:264–271

Xu G, Liang S, Fan J, Sheng G, Luo X (2016) Amperometric sensing of nitrite using a glassy carbon electrode modified with a multilayer consisting of carboxylated nanocrystalline cellulose and poly(diallyldimethyl ammonium) ions in a PEDOT host. Microchim Acta 183:2031–2037

Yang H, van de Ven TGM (2016) A bottom-up route to a chemically end-to-end assembly of nanocellulose fibers. Biomacromol 17:2240–2247

Yang H, Tejado A, Alam N, Antal M, van de Ven TGM (2012) Films prepared from electrosterically stabilized nanocrystalline cellulose. Langmuir 28:7834–7842

Yang X, Xie H, Du H, Zhang X, Zou Z, Zou Y, Liu W, Lan H, Zhang X, Si C (2019) Facile extraction of thermally stable and dispersible cellulose nanocrystals with high yield via a green and recyclable FeCl3-catalyzed deep eutectic solvent system. ACS Sustain Chem Eng 7:7200–7208

Zhang YHP, Cui J, Lynd LR, Kuang LR (2006) A transition from cellulose swelling to cellulose dissolution by o-phosphoric acid: evidence from enzymatic hydrolysis and supramolecular structure. Biomacromol 7:644–648

Zou X, Tan X, Berry R, Godbout JDL (2016) Flexible, iridescent nanocrystalline cellulose film, and method for preparation, Google Patents